Crossed molecular beams and quasiclassical trajectory studies of the reaction O (1 D)+ H 2 (D 2)

M. Alagia, N. Balucani, L. Cartechini, P. Casavecchia, E. H. van Kleef, G. G. Volpi, P. J. Kuntz, and J. J. Sloan

Citation: The Journal of Chemical Physics **108**, 6698 (1998); doi: 10.1063/1.476085
View online: http://dx.doi.org/10.1063/1.476085
View Table of Contents: http://scitation.aip.org/content/aip/journal/jcp/108/16?ver=pdfcov
Published by the AIP Publishing

Crossed molecular beams and quasiclassical trajectory studies of the reaction $O(^1D)+H_2(D_2)$

M. Alagia, N. Balucani, L. Cartechini, P. Casavecchia, E. H. van Kleef, and G. G. Volpi
Dipartimento di Chimica, Università di Perugia, 06123 Perugia, Italy

P. J. Kuntz
Hahn-Meitner-Institute fur Kernforschung Berlin, D-1000 Berlin 39, Germany

J. J. Sloan
Department of Chemistry, University of Waterloo, Waterloo, Canada N2L 3G1

(Received 10 October 1997; accepted 22 January 1998)

The dynamics of the reactions $O(^1D)+H_2\rightarrow OH+H$ and $O(^1D)+D_2\rightarrow OD+D$ have been investigated in crossed molecular beam experiments with mass spectrometric detection at the collision energies of 1.9 and 3.0 kcal/mol, and 5.3 kcal/mol, respectively. From OH(OD) product laboratory angular and velocity distribution measurements, center-of-mass product translational energy and angular distributions were derived. The angular distributions are nearly backward–forward symmetric with a favored backward peaking which increases with collision energy. About 30% of the total available energy is found to be channeled into product translational energy. The results are compared with quasiclassical trajectory calculations on a DIM (diatomic-in-molecules) potential energy surface. Related experimental and theoretical works are noted. Insertion via the $1\,^1A'$ ground state potential energy surface is the predominant mechanism, but the role of a second competitive abstraction micromechanism which should evolve on one of (or both) the first two excited surfaces $^1A''$ and $2\,^1A'$ is called into play at all the investigated energies to account for the discrepancy between theoretical predictions and experimental results. © *1998 American Institute of Physics.* [S0021-9606(98)01116-7]

I. INTRODUCTION

The reaction $O(^1D)+H_2(^1\Sigma_g^+)\rightarrow OH(X\,^2\Pi;v',J')+H(^2S)$, $\Delta H^\circ_0=-43.4$ kcal/mol, and its deuterated analogs have received a great deal of attention due to their fundamental and practical importance. About 15 years ago, when the first measurements of the internal energy distributions of the OH product became available,[1–6] it was realized that the dynamics of this reaction differs remarkably from those of the prototypical hydrogen–halogen reactions which had provided many of the basic concepts of modern reaction dynamics. Most of the early experiments were interpreted in terms of a reaction mechanism which involves the insertion of the $O(^1D)$ atom into the H_2 bond, with the transitory formation of ground state $H_2O(\tilde{A}\,^1A_1)$, but none proved this unequivocally. A few of the early experimental results were thought to indicate that abstraction also contributes to the reaction.

The rotational distributions in the low-v' states of the $OH(X\,^2\Pi;v',J')$ product were found to be strongly inverted, reaching to the maximum energetically allowed values,[1–3,6] but this observation gave little dynamical information, since it was shown subsequently to be primarily the result of angular momentum constraints.[7–10] The earliest measurements of the angular distribution[11] showed symmetric forward–backward peaking of the product OH, but this is not necessarily related to the formation of a long-lived complex: it may simply indicate that, due to the symmetry of the H–O–H intermediate, the central O atom interacts equally with both H atoms and, therefore, the bond breaking probability is the same for the two O–H bonds. The OH vibrational distribution obtained by combining the results of infrared chemiluminescence (IC),[4,5] laser induced fluorescence (LIF),[12–15] and chemical laser (CL)[16] measurements has similar populations for the $v'=0-3$ levels and a substantially lower population for the highest accessible level, $v'=4$. This distribution does not give unequivocal information about the dynamics either, since it is neither strongly inverted, which would be expected from collinear direct abstraction dynamics, nor monotonically decreasing with v', which would result from the formation of a long-lived H–O–H intermediate.

A large number of quasiclassical trajectory (QCT)[17–21] and quantum mechanical[22,23] scattering calculations on this reaction were carried out as well. Most of these were done at low kinetic energy, using either the Schinke and Lester[24] or Murrell and Carter[25] potential energy surfaces (PESs), both of which are single-valued approximations to the lowest energy surface. These calculations concluded that the reaction is predominantly an insertion, but the experimental product vibrational distribution was not well predicted in any of them. A more recent QCT calculation[26] using a much improved (but still single valued) surface based on new high-quality *ab initio* computations, gave better agreement with some of the experimental data. This latter calculation also concluded that the majority of the trajectories are insertions, and, more importantly, that the product angular distributions for $O(^1D)+H_2$ at relative translational energies of 0.5 and 5.0 kcal/mol are backward–forward symmetric. A new

single-valued potential energy surface for H_2O based on an energy switching approach which has spectroscopic accuracy in certain regions has been recently proposed by Varandas[27] and used in dynamics calculations.[28]

It is not possible in principle for a single-valued surface to reproduce the behavior of this system, since $O(^1D)$ and $H_2(X\ ^1\Sigma_g^+)$ correlate with the observed products, $OH(X\ ^2\Pi)$ and $H(^2S)$, *via* two surfaces of differing (A' and $^1A''$) symmetry, and these surfaces have conical intersections with a third surface of $^1A'$ symmetry, which correlates with $OH(A\ ^2\Sigma)+H(^2S)$. The conical intersections are accessible at the energies of the experiments, and the approximations used by single-valued surfaces in these regions can introduce unphysical features, which distort trajectories.

We have previously done several different QCT studies on the $O(^1D)+H_2(X\ ^1\Sigma^+g)$ system, using a multisurface DIM (diatomic-in-molecules) model,[29] which explicitly includes the conical intersections. Our model has complete descriptions of all five possible potential energy surfaces, of which the lowest three are relevant at the energies of the experiments. The two lowest $^1A'$ surfaces ($1\,^1A'$, denoted eig. 1 and $2\,^1A'$, denoted eig. 2) were included in our QCT studies,[30] and a surface-hopping algorithm in the code permitted the system to access both. The ground state surface has no barrier for either C_{2v} insertion of the $O(^1D)$ into the H–H bond (leading to the ground state of H_2O) or collinear reaction (where $^1A'$ becomes the $^1\Sigma$ state). The next higher $^1A'$ surface (eig. 2) is repulsive, especially in C_{2v} configurations, where it leads to the $^1B_2$ state of H_2O. In collinear geometry, this surface ($2\,^1A'$) correlates with the products $OH(X\ ^2\Pi)+H(^2S)$ and forms one of the components of the doubly degenerate $^1\Pi$ state (the other Renner–Teller component is the first $^1A'$ state), which has a barrier of 3.7 kcal/mol to reagent approach in this potential model. Our calculations showed that the dynamics of reactions which hop from the lower to the upper surface[31] or which occur completely on the upper surface[32] differ dramatically from those which occur only on the lower surface. In particular, reactions which occur completely on the excited state surface give strongly inverted vibrational distributions, and backward peaked angular distributions, as expected from abstraction dynamics. Thus single-surface calculations which ignore these possibilities are at risk of neglecting important dynamical effects.

The role of the $^1A'$ surface has been recently explored by Schatz *et al.*,[33] who have derived, in addition to the ground state surface, a high-quality *ab initio* excited state $^1A''$ PES, and have included it in an adiabatic fashion in QCT calculations. The results obtained by Schatz *et al.*[33] on the $^1A''$ surface are qualitatively similar to those of DIM calculations on the excited state PES $2\,^1A'$ by Kuntz *et al.*,[32] since they also find an inverted vibrational distribution and a strongly backward peaked angular distribution as a consequence of direct abstraction. Noticeably, the barrier for direct abstraction is 2.3 kcal/mol on the new $^1A''$ PES, so that contribution to the dynamics from direct abstraction is expected to occur at significantly lower relative translational energies than in the DIM PES. A double valued surface has also been proposed by Varandas,[34] but it has not been used in dynamic computations yet. Very recently, Schatz *et al.*[35] have examined in some detail the contribution of both excited electronic states ($^1A''$ and $2\,^1A'$) and the coupling between the ground and the excited states in the reaction dynamics using DIM PES and couplings.

New measurements of the $O(^1D)+H_2$ rate constants,[36–39] as well as the OD/OH branching ratios[38–40] and product angular and translational energy distributions[41] for the $O(^1D)+HD$ reaction have appeared. The new data do not change the qualitative picture which the previous work produced, but certain findings require further theoretical treatment. In particular, the new OD and OH angular and translational energy distributions, measured in crossed pulsed beam experiments using Doppler-shift techniques in a REMPI (resonance enhanced multiphoton ionization) detection scheme of the $H(D)$ atom, contain additional dynamical information, as the symmetry of the H–O–H intermediate is broken in this case. At the reagent translational energy $E_c = 4.55$ kcal/mol, the OD peaks at higher translational energy than the OH and both exhibit predominantly backward scattering.[41] The experimental results are not consistent with a simple insertion mechanism, and the suggestion was made that either the conical intersections have an effect or there is a component of abstraction in the dynamics.[41] An attempt to theoretically interpret these findings has been reported by Schatz and co-workers[33] by considering in their calculations also the first $^1A''$ surface; however, when the contribution of this surface is added to the ground state angular distribution, which reflects insertion dynamics, a significant underestimate of the experimental backward scattering is still observed. Interestingly, it was noted that the $^1A''$ barrier in the *ab initio* PES is perhaps too high by 1 kcal/mol; but calculations which mimic the effect of lowering the $^1A''$ barrier did not lead to an improved agreement with the experiment, since they showed that the $^1A''$ integral cross section increases, but the backward peak in the angular distribution broadens without increasing in intensity.[33] Very recently, Hsu and Liu[42] have reported improved results for the $O(^1D)+HD$ reaction at $E_c = 4.53$ kcal/mol by using the Doppler-selected time-of-flight method to derive differential cross sections under higher resolution conditions, and these results essentially confirm the previous findings.[41]

Liu and co-workers[43] have provided additional direct evidence for the abstraction pathway from measurements of the dependence of the integral cross sections on the collision energy in the range from 0.6 to nearly 6 kcal/mol for $O(^1D)+H_2$, D_2, and HD. A reaction barrier of about 1.8 kcal/mol was inferred for the abstraction channel. Furthermore, the OD/OH branching ratio as a function of relative translational energy confirmed the presence of two competitive micromechanisms. Again, QCT calculations,[33,35] including both ground $^1A'$ and first two excited PESs, $^1A''$ and $2\,^1A'$, are not in agreement with the crossed beam results as far as the shape of the energy dependence of the integral reactive cross section (i.e., excitation function) for $O(^1D)+H_2$, D_2, HD and of the branching ratio for $O(^1D)+HD$ are concerned.

By using the new experimental strategy of polarized-laser-photolysis and polarized sub-Doppler LIF detection in

a bulb, Simons and co-workers[44] derived the state-resolved differential cross section for $O(^1D)+H_2 \rightarrow OH(X\ ^2\Pi_{3/2};\ v'=0,\ N=5)$ at a mean collision energy of 2.4 kcal/mol. For this particular product state, which was found to be strongly backward scattered, QCT predictions on only the ground state surface [a modified version of the Schinke–Lester (SL1) surface][45] were in qualitative agreement with the experimental observation. Very recently, the reaction $O(^1D)+D_2$ has also been investigated by Suits and co-workers[46] using ion-imaging techniques in a pulsed crossed beams arrangement.

Despite all the current experimental and theoretical effort, the detailed dynamics of $O(^1D)+H_2$ continue to be a challenge. In particular, experimental and theoretical confirmations of the role of the second competitive micromechanism and/or of the effect of the conical intersections are needed. In order to shed more light on the complicated dynamics of this reaction, we have carried out high-resolution angular and translational energy distribution measurements by using the crossed molecular beam (CMB) scattering method with rotating mass spectrometric detection. Here, we report the results we obtained on $O(^1D)+H_2$ at $E_c=1.9$ and 3.0 kcal/mol and on $O(^1D)+D_2$ at $E_c=5.3$ kcal/mol. We have also carried out QCT calculations at the energies of the experiments, using a multisurface DIM model and beginning on the lowest surface (eig. 1), since the barrier of 3.7 kcal/mol to direct abstraction on the first two excited surfaces of this model prevents a significant contribution from this micromechanism at the present energies (see Sec. III). The purpose is to carry out direct comparisons with experimental results and to assess the reliability of the present DIM potential model.

The experiments will be described in Sec. II and the QCT calculations in Sec. III. The experimental and QCT results are compared in Sec. IV and discussed in Sec. V. Conclusions follow in Sec. VI.

II. EXPERIMENTAL RESULTS AND ANALYSIS

A. The crossed molecular beam experiments

The experiments were carried out by using a crossed molecular beam apparatus that has been described in detail elsewhere.[47,48] Briefly, two well collimated supersonic beams of the reagents are crossed at 90° in a large scattering chamber with background pressure in the 10^{-7} mbar range, which assures the single collision conditions, and a mass spectrometer, contained in a triply differentially pumped ultrahigh-vacuum chamber, serves as detector of the reaction products. The mass spectrometer can be rotated in the collision plane around an axis passing through the collision center and the velocities of the particles can be derived from time-of-flight (TOF) measurements. In the present experiments a selection of the velocities as well as a partial selection of the internal quantum states of the reactants by supersonic expansion is achieved. The selection of the translational energy of the products also gives (by energy conservation) their internal (rotational plus vibrational) energy.

The detection system consists of an electron bombardment ionizer, a quadrupole mass filter and an off-axis (90°) secondary electron multiplier. The ionizer is located in the innermost region of the detector which is maintained in the 10^{-11} mbar pressure range in operating conditions by extensive ion-, turbo-, and cryo-pumping. The extensive pumping and cooling are essential in these experiments where the product mass ($m/e=17$) is strongly affected by the inherent background of water.

The two beam sources are usually doubly differentially pumped; however, for the present experiments, the secondary molecular (H_2,D_2) beam source was brought close to the collision region, with only one stage of differential pumping, to gain intensity. This beam source is pumped by 4200 and 2400 *l*/s diffusion pumps, while the oxygen atom source features a 6000 *l*/s diffusion pump and a 2400 l/s differential diffusion pump; both beam sources are backed by 500 m^3/h roots pumps.

The supersonic atomic oxygen beams, containing both the ground state $O(^3P)$ and the electronically excited $O(^1D)$, were generated by the high-pressure radio-frequency (RF) discharge beam source successfully used in our laboratory over a number of years to generate intense supersonic beams of atoms and radicals.[49–51] The oxygen beams contain a small percentage of $O(^1D)$ and a very large fraction of ground state $O(^3P)$,[49] but this species does not interfere as the collision energies of our experiments are not high enough to overcome the energy barrier of the reaction $O(^3P)+H_2 \rightarrow OH+H$, which is known to be more than 8 kcal/mol. This source, which is similar in design to that described by Sibener *et al.*[52] and which has been optimized for $O(^1D)$ production, has been discussed in some detail elsewhere.[48–50] Briefly, high levels of RF power are fed, through an LC circuit made to resonate around 14 MHz, into a plasma contained in a quartz nozzle (orifice diam 0.24 mm) cooled with low electrical conductivity water. We start from a dilute mixture (a few percent) of O_2 in He or Ne gas. The plasma is directly localized behind the orifice of the nozzle, which permits achieving a high degree of molecular dissociation (about 95% with 5% O_2–Ne gas mixtures and about 80% with 5% O_2–He mixtures). The beam is skimmed by a boron nitride skimmer (diam 1.0 mm) located at a distance of 5.2 mm from the nozzle and further collimated by a rectangular slit. By discharging 250 mbar of 5% O_2 in Ne with a RF power of 325 W, a peak velocity of 1573 m/s and a speed ratio of 5.9 were obtained. By discharging 385 mbar of 5% O_2 in He at 350 W, the peak velocity and speed ratio were 2780 m/s and 6.1, respectively. These two mixtures were used for the study of the $O(^1D)+H_2$ reaction, giving canonical collision energies of 1.9 and 3.0 kcal/mol, respectively. The angular divergence was 2.3° for the low energy experiment and 1.5° for the high energy one. Instead, for the $O(^1D)+D_2$ system, in order to improve the signal-to-background ratio, a 4% mixture in He of isotopically enriched oxygen (50% $^{18}O_2$, 50% $^{16}O_2$) was used to generate a beam of ^{18}O. This allowed us to detect the ^{18}OD product at $m/e=20$, which has a very low inherent background in the detector. Operating conditions were 350 mbar of pressure and 300 W of RF power, which gave a peak velocity of 2670

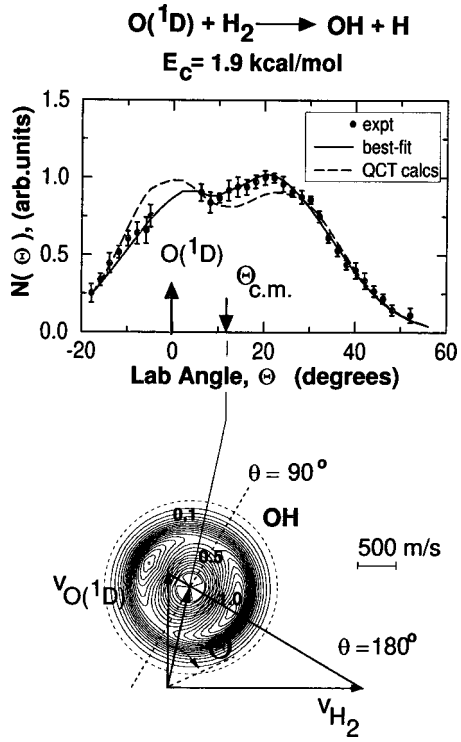

FIG. 1. Laboratory OH angular distribution for the $O(^1D)+H_2$ reaction at $E_c=1.9$ kcal/mol and c.m. product flux contour map superimposed on the most probable Newton diagram. Solid line: calculated curve with best-fit center-of-mass angular and translational energy distributions. Dashed line: QCT prediction.

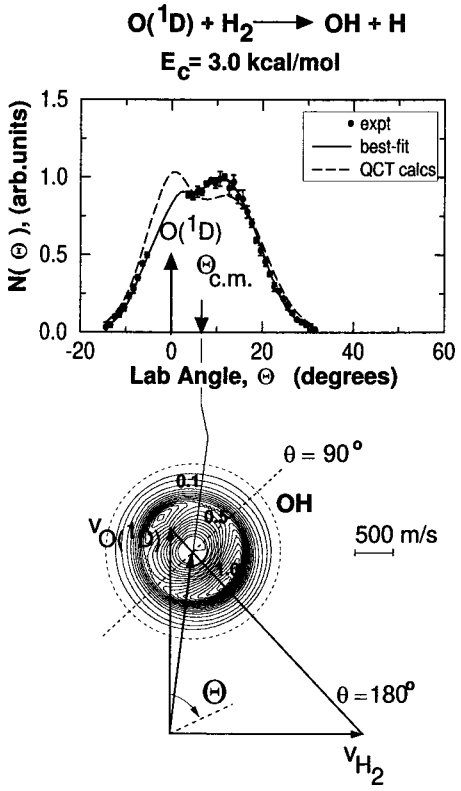

FIG. 2. As in Fig. 1, but at $E_c=3.0$ kcal/mol.

m/s, a speed ratio of 6.3, and a collision energy of 5.3 kcal/mol.

The beam of H_2 was produced by supersonic expansion of pure H_2 at a stagnation pressure of 2.5 bar through a 70-μm stainless-steel nozzle kept at room temperature, while the beam of D_2 was generated by expanding pure D_2 at a pressure of 4 bar and with the nozzle resistively heated at 573 K in order to increase the beam translational energy. Peak velocity and speed ratio were 2610 m/s and 18.0 for the H_2 beam and 2620 m/s and 13.2 for the D_2 beam. With only one stage of differential pumping, the beam angular divergence was about 5°. Experiments carried out using doubly differentially pumped H_2 beams with 2.3° angular divergence gave identical results and simply lower signal intensity as a consequence of the longer distance between the nozzle and the collision center. The rotational temperatures of the n-$H_2(j)$ and n-$D_2(j)$ reagent molecules in the beams under the expansion conditions were estimated by extrapolating the consistent experimental determinations of Pollard *et al.*[53] For the H_2 beam, the corresponding relative rotational populations are 0.18, 0.75, and 0.07 for $j=0,1$ and $j\geqslant 2$, while for the D_2 beam the populations are 0.23, 0.26, 0.37, and 0.14 for $j=0,1,2$, and $j\geqslant 3$, respectively. We recall that the rotational energies of the $j=1$ and 2 states of H_2 are 0.35 and 1.03 kcal/mol, respectively, while those of the $j=1,2$, and 3 states of D_2 are 0.17, 0.51, and 1.03 kcal/mol.

The laboratory angular distributions of the OH(OD) product, $N(\Theta)$, are obtained by taking several scans of 50 s counts at each angle. The nominal angular resolution of the detector for a point collision zone is 1°. The secondary target beam (in the present experiment the H_2/D_2 beam) is modulated at 160 Hz by a tuning fork chopper. The background and signal plus background counts are obtained from a pulse counting dual scaler, synchronously gated with the tuning fork. Because of the presence in the oxygen beam of naturally abundant ^{17}O and because of a very small mass 16 leakage to $m/e=17$, a small correction for the contribution of elastically scattered signal detected at $m/e=17$ had to be brought to the measured angular distributions for $O(^1D)+H_2$ at angles close to the oxygen beam in order to obtain the pure reactive distributions. The small elastic contamination was quantified by measuring the angular distribution of $m/e=16$ elastically scattered from H_2 and by verifying that the elastic $m/e=16$ and 17 angular distributions obtained by scattering from a beam of pure He were the same.

The reactant beam velocities are measured by single-shot TOF analysis using a standard disk (four slits, 0.3 mm wide on a 145-mm-dia disk, thickness 0.1 mm, 300 Hz), located at the entrance of the detector and positioning the detector (equipped with a 0.3-mm diameter entrance slit) in axis with the beam. Product velocity distributions, $N(\Theta,v)$, are obtained at selected laboratory angles using the cross-correlation TOF technique:[54] a pseudorandom chopper (145-mm diam, 0.1-mm thick) with four 127-bit pseudorandom sequences (slit width about 0.9 mm) was spinned at 328.1 Hz, corresponding to a dwell time of 6 μs/channel. For the TOF measurements a high-speed multichannel scaler and a computer-controlled CAMAC data acquisition system was used. The flight length was 24.5 cm. Counting times were of 30–60 min.

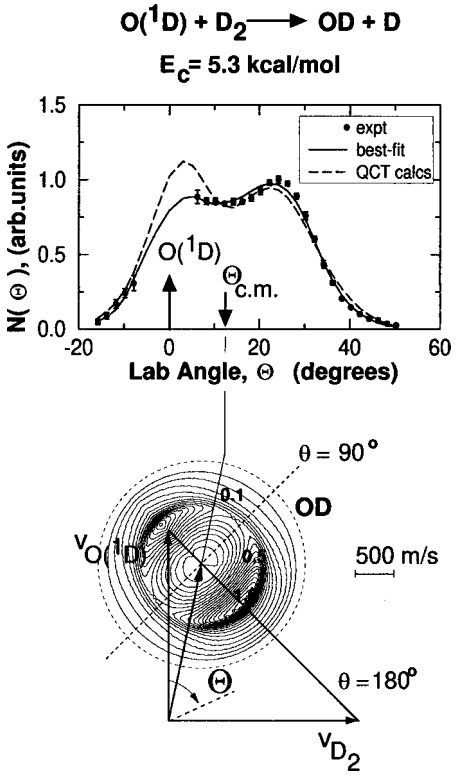

FIG. 3. As in Fig. 1, but for $O(^1D)+D_2$ at $E_c=5.3$ kcal/mol.

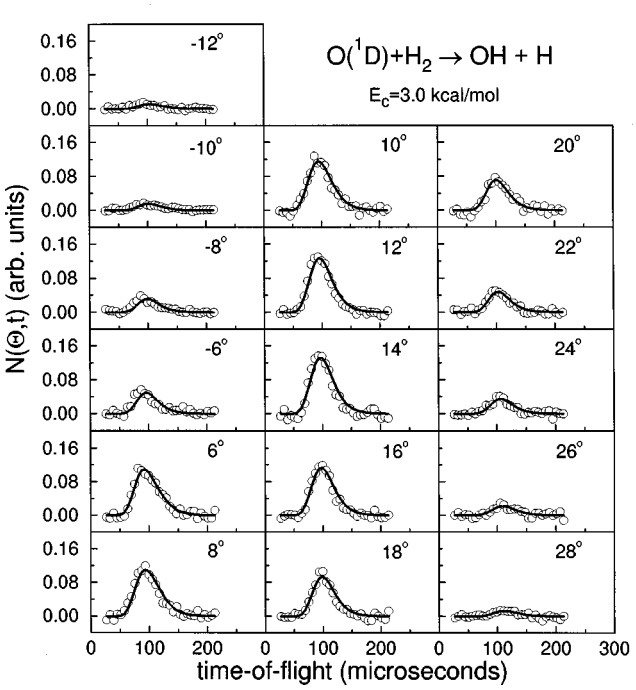

FIG. 5. TOF spectra of the OH product for the $O(^1D)+H_2$ reaction at $E_c=3.0$ kcal/mol.

The lab product angular distributions from the $O(^1D)+H_2$ reaction at $E_c=1.9$ and 3.0 kcal/mol and from the $^{18}O(^1D)+D_2$ reaction at $E_c=5.3$ kcal/mol are shown in Figs. 1–3, together with the canonical Newton diagrams. The error bars are indicated representing ± 1 standard deviation. The solid and dashed curves are best-fit and QCT calculations, respectively, as described in Secs. II B and III. The contour maps superimposed on the Newton diagrams are described in Sec. II B. The TOF distributions at selected lab angles are shown in Figs. 4–6.

B. Analysis of the experimental results

For the physical interpretation of the scattering results it is necessary to transform the angular, $N(\Theta)$, and velocity, $N(\Theta,v)$, distributions measured in the laboratory coordinate system to the center-of-mass reference frame. This transformation is fairly straightforward and the relation between lab and c.m. fluxes is given by

$$I_{\text{lab}}(\Theta,v)=I_{\text{c.m.}}(\theta,u)v^2/u^2, \tag{1}$$

i.e., the scattering intensity observed in the laboratory is distorted by the transformation Jacobian v^2/u^2 from that in the c.m. system, where v and u are lab and c.m. velocities, respectively. Since an electron impact ionization mass spectrometric detector measures the number density of products, $N(\Theta)$, and not their flux, the actual relation between the lab density and the c.m. flux is given by

$$N_{\text{lab}}(\Theta,v)=I_{\text{c.m.}}(\theta,u)v/u^2. \tag{2}$$

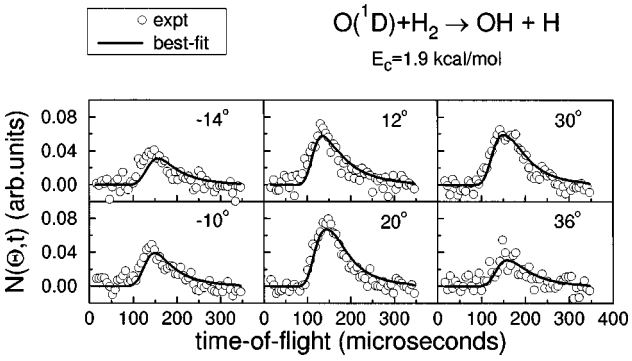

FIG. 4. TOF spectra of the OH product for the $O(^1D)+H_2$ reaction at $E_c=1.9$ kcal/mol.

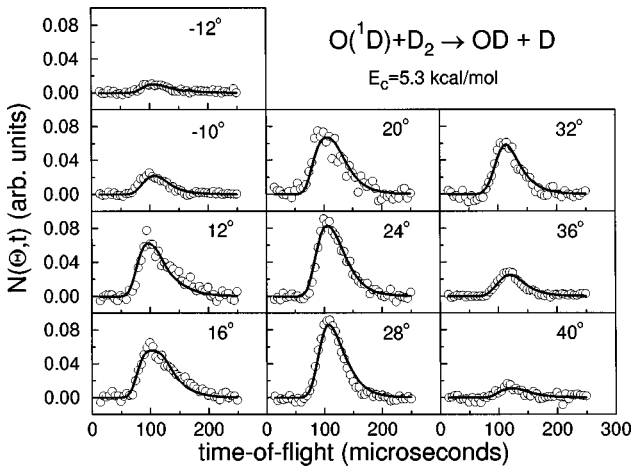

FIG. 6. TOF spectra of the OD product for the $O(^1D)+D_2$ reaction at $E_c=5.3$ kcal/mol.

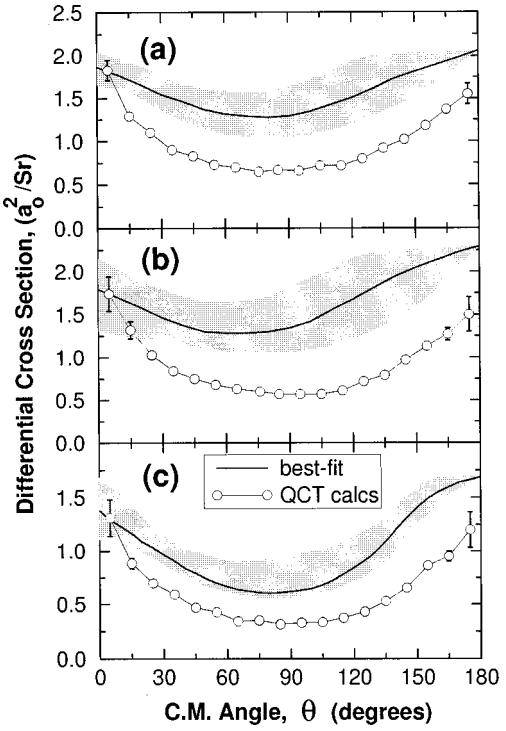

FIG. 7. (a) Solid line: c.m. product angular distribution for $O(^1D)+H_2$ at $E_c=1.9$ kcal/mol with error bars (shaded area); open circles: QCT prediction; (b) as in (a), but at $E_c=3.0$ kcal/mol; (c) as as in (a), but for $O(^1D)+D_2$ at $E_c=5.3$ kcal/mol.

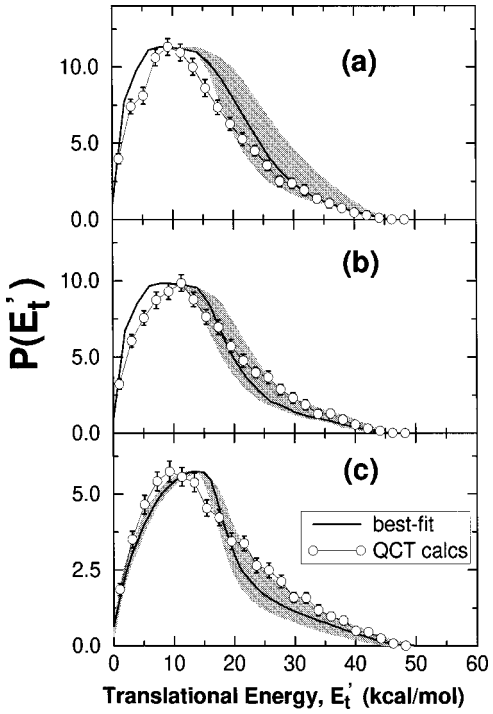

FIG. 8. (a) Solid line: product translational energy distribution for $O(^1D)+H_2$ at $E_c=1.9$ kcal/mol with error bars (shaded area); open circles: QCT prediction; (b) as in (a), but at $E_c=3.0$ kcal/mol; (c) as in (a), but for $O(^1D)+D_2$ at $E_c=5.3$ kcal/mol.

Because of the finite resolution of experimental conditions, analysis of the laboratory data is carried out, as usual, by forward convolution procedures over the experimental conditions of trial c.m. distributions. The final outcome is the generation of a velocity flux contour map of the reaction products, i.e., the plot of the intensity as a function of angle and velocity in the c.m. system, $I_{\text{c.m.}}(\theta,u)$. The contour map can be regarded as an *image* of the reaction (see Figs. 1–3).

The fit of product angular distributions and TOF spectra was attempted by a forward convolution trial-and-error procedure that assumes a separable form for the c.m. frame product flux distribution $I_{\text{c.m.}}(\theta,E')=T(\theta)P(E')$, where the $T(\theta)$ function represents the c.m. total differential cross section and $P(E')$ is the product translational energy distribution. The energy dependence of the integral reactive cross section, as recently determined by Liu and co-workers,[43] has been included in the data analysis; the effect was negligible, however, because of the narrow spread of relative translational energies in these experiments. The continuous lines in Figs. 1–6 are the lab angular and TOF distributions calculated from the best-fit c.m. angular and translational energy distributions, which are depicted as a solid line in Figs. 7 and 8; the hatched areas in Figs. 7 and 8 delimit the range of c.m. functions which still afford an acceptable fit to the data, i.e., they represent the error bars of the present determination. As can be seen in Figs. 1, 2, 4, and 5, the lab OH angular and TOF distributions are well reproduced, and this indicates that for $O(^1D)+H_2$ the coupling between the product angular and translational energy distributions is weak within the sensitivity of our data. In the case of $O(^1D)+D_2$, the backward peak in the OD angular distribution (Fig. 3) is not well reproduced; an improved fit of the OD lab angular distribution (not shown here) could be obtained by accounting for the coupling of $P(E')$ and $T(\theta)$, and using a less energetic $P(E')$ in the sideways direction.

The best-fit c.m. functions are also reported as product flux (velocity-angle) contour maps in Figs. 1–3 superimposed on the Newton diagrams. The contour maps highlight the features inferred from the lab angular distributions; in fact, from them one can immediately see how the OH(OD) angular distribution is distributed over all the angular range with peaks at $\theta=180°$ (backward) and $\theta=0°$ (forward), but exhibits a somewhat preferential backward scattering. The position of the peak in the c.m. velocity scale reflects the fraction of total available energy released as product translational energy and this mirrors, by energy conservation, the product internal (vibrational+rotational) energy distribution.

The average product translational energy,

$$\langle E_t' \rangle = \Sigma_{E'} P(E_t') E_t' / \Sigma_{E'} P(E_t'), \tag{3}$$

is 14.3 and 13.2 kcal/mol for $O(^1D)+H_2$ at $E_c=1.9$ and 3.0 kcal/mol, that is, 31.6% and 28.4%, respectively, of the total available energy (the total available energy is given by the sum of the collision energy and of the reaction exothermicity). $\langle E_t' \rangle$ is 14.0 kcal/mol for $O(^1D)+D_2$ at $E_c=5.3$ kcal/mol, which corresponds to 29.0% of the total energy. This modest fraction of energy released as translational motion of the products points to a high internal (rovibrational) excitation, as predicted by IC, CL, and LIF studies,[4,5,12–16] and as also found in other CMB experiments[11,41,42,44,46] on the various isotopic variants of this reaction.

Comparison with previous experimental findings is in order. The CMB study of Buss *et al.*[11] on $O(^1D)+H_2$ at $E_c=2.7$ kcal/mol, a value close to the higher collision energy of the present study, found a symmetric c.m. angular distribution and a fraction of energy released as product recoil energy of about 32%. We attribute the difference with respect to what is derived here to the lower angular and TOF resolution of the earlier study. In particular, in the present experiment we have been able to explore the product distribution closer to the $O(^1D)$ beam than in the earlier study. It should be noted that the lab angular range in the vicinity of the oxygen beam, which corresponds to the forward direction of the product in the c.m. frame, cannot be fully explored in this type of experiment, which uses a mass spectrometer detector.

The main features of the experimental results in Figs. 7 and 8 are qualitatively similar to those of the corresponding distributions reported recently[41,42] for the $O(^1D)+HD$ reaction. That experiment also showed a preference for backward scattering of both the OH and OD. We note that the product translational energy distribution for the $O(^1D)+HD$ reaction at $E_c=4.53$ kcal/mol peaks around a relatively low value of product translational energy, ~ 6 for the OH+D channel and ~ 9 cal/mol for the OH+H channel[see Fig. 3(a) of Ref. 42 and Fig. 2(a) of Ref. 41], while the distributions derived here for $O(^1D)+H_2$ at $E_c=3.0$ and for $O(^1D)+D_2$ at $E_c=5.3$ kcal/mol peak around values considerably larger, ~ 10 and $\sim 13-14$ kcal/mol, respectively. At the same time, we note that the product c.m. angular distribution for the $O(^1D)+HD\rightarrow OH+D$ reaction exhibits a very pronounced degree of polarization (i.e., the intensities at $\theta=0$ and 180° are much higher—by about a factor five—than at $\theta=90°$), which is considerably larger than that observed in the present experiments. It remains to be seen if these differences can be ascribed to the peculiarity of the asymmetric $O(^1D)+HD$ system. Liu's group[55] has recently determined differential cross sections, besides those for $O(^1D)+HD$, also for $O(^1D)+H_2$ and D_2 at energies comparable to ours, but the results have not been published yet.

The experimental results of Simons and co-workers on $O(^1D)+H_2$ at $E_c=2.4$ kcal/mol refer to a specific rotational state of the ground vibrational level of the OH product and, therefore, cannot be directly compared with the present results.

III. QUASICLASSICAL TRAJECTORY CALCULATIONS

QCT calculations were carried out on a potential energy surface which is an extension of the DIM model which was described in Ref. 29. The main properties of the current model, revision 5, are reported in Ref. 32. It contains all the surfaces which correlate with $O(^1D)+H_2(X\ ^1\Sigma^+g)$, but for the calculations of Refs. 30–32, only those of A' symmetry (in C_s configurations) were used. Of these, the lowest energy surfaces are treated more accurately than the higher ones, because they are more important for the (mostly low-energy) experiments. This model gives good agreement with experimental kinetics and themochemistry. It predicts that the total rate constant (taking into account the fivefold electronic degeneracy in the entrance channel) at 300 K is $k=1.92\times 10^{-10}$ cm^3 s^{-1} in molecular units (the experimental value[38] is $k(298)=1.2\pm 0.1\times 10^{-10}$ cm^3 s^{-1}). For the surfaces leading from $O(^1D)+H_2(X\ ^1\Sigma^+g)$ to $H(^2S)+OH(X\ ^2\Pi)$, the exothermicity, defined as the difference from the minimum of the $H_2(X\ ^1\Sigma^+g)$ potential to the minimum of the $OH(X\ ^2\Pi)$ potential, is -42.57 kcal/mol.

For $O(^1D)+H_2$, we have calculated five batches of 20 000 trajectories, each at reagent translational energies (E_c) of 2.0, 3.0, 4.0, and 5.5 kcal/mol. This range of energies includes the experimental measurements and also is wide enough to identify the energy dependent trends on the ground state surface. In addition to these, we calculated batches of 20 000 trajectories for the $O(^1D)+D_2$ reaction at $E_c=5.3$ kcal/mol and for $O(^1D)+HD$ at $E_c=4.55$ kcal/mol. The former is directly comparable with the $O(^1D)+D_2$ experiment reported above; the latter is for comparison with the results reported in Ref. 41. At all the investigated energies, the contribution to the reactive scattering from trajectories started on the excited $2\ ^1A'$ PES is expected to be negligible, as shown in previous work,[32] where a significant contribution was found for $O(^1D)+H_2$ starting at $E_c=6.9$ kcal/mol.

IV. COMPARISON BETWEEN SCATTERING AND QCT RESULTS

The experimental c.m. angular distributions for $O(^1D)+H_2$ at $E_c=1.9$ and 3.0 kcal/mol are shown as a solid line in Figs. 7(a) and 7(b), where are compared with the QCT results for $E_c=2.0$ and 3.0 kcal/mol indicated by the circles. The experimental and QCT c.m. angular distributions for $O(^1D)+D_2$ at $E_c=5.3$ kcal/mol are shown in Fig. 7(c). In Figs. 7(a)–7(c), the experimental results (relative units) and the QCT results (a_0^2/sr) are normalized at $\theta=0°$. The error bars on the QCT results, which indicate the uncertainty at the 95% confidence level, are smaller than the plotted symbols except for the extreme ends of the plots, where they are visible. The shapes of the QCT angular distributions are very nearly the same for all energies, but the cross sections for $O(^1D)+H_2$ decrease with increasing energy.

The experimental distributions have nearly equal intensity at $\theta=0$ and $\theta=180°$, but they show a distinct excess intensity in the backward hemisphere with the backward peak somewhat broad, from which we conclude that the angular distributions for $O(^1D)+H_2$ and D_2 are not exactly forward–backward symmetric, as indicated by earlier work.[11] A slight increase of the backward–forward asymmetry with increasing E_c is noted for $O(^1D)+H_2$. On the contrary, within the statistical uncertainty of the calculation, the QCT angular distributions are essentially forward–backward symmetric with a small excess in the forward direction.

Figure 8 shows the product translational energy distributions which correspond to the angular distributions of Fig. 7. The QCT calculations for $O(^1D)+H_2$, indicated by the circles, peak approximately at the same product energy as the experiments, about 10 kcal/mol, have similar shape, and decrease smoothly to the limit of the available energy. However, some discrepancies are noticeable in the peak positions and tails of the distributions.

The comparison can be made more directly by simulat-

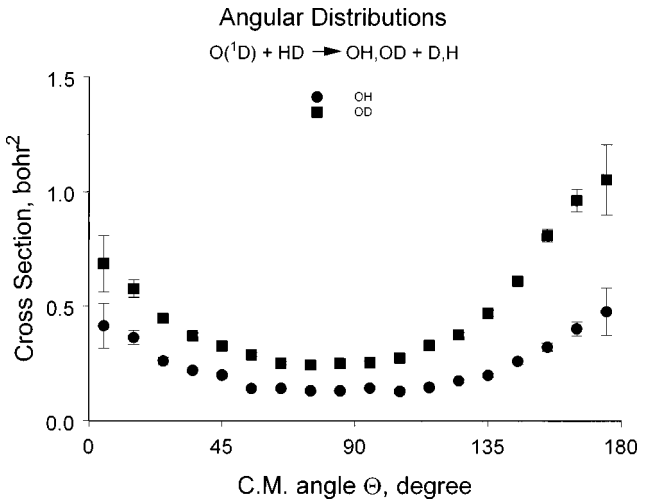

FIG. 9. QCT results for OH (circles) and OD (squares) c.m. angular distributions for the $O(^1D)+HD$ reaction at $E_c=4.55$ kcal/mol.

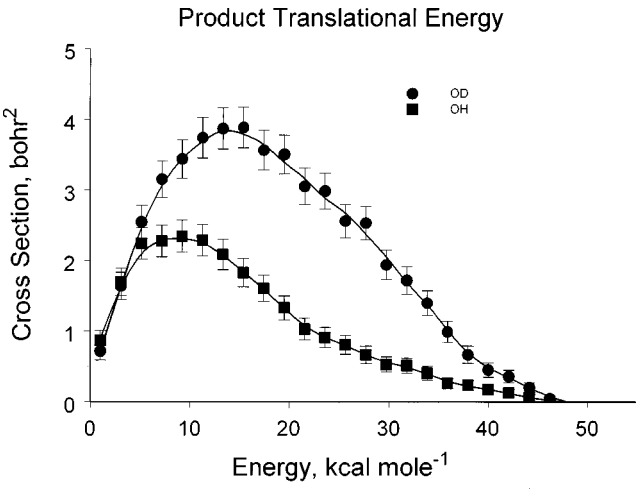

FIG. 10. QCT results for the product translational energy distributions for the $O(^1D)+HD$ reaction at $E_c=4.55$ kcal/mol. Circles: OD channel, squares: OH channel.

ing the lab angular distributions using the QCT results of Figs. 7 and 8. The QCT simulation is the dashed line in Figs. 1–3. As can be seen, the QCT c.m. functions (Fig. 7) generate forward–backward asymmetry ratios in the lab angular distributions opposite to those which are experimentally observed: this is mainly a consequence of the symmetric shapes of the QCT c.m. angular distributions. The simulated distributions are also slightly broader than the experiments, especially at the higher E_c: this can be attributed to the fact that the QCT translational energy distributions are slightly hotter than the experiment.

The experiments of Liu and co-workers[41,42] on $O(^1D)+HD$ showed a preference for backward scattering of both the OH and OD and, in addition, that the reagent masses also influence the dynamics. The backward/forward intensity ratio of the OD was reported to be greater than 3, while that of the OH was about 1.7 (the more recent high-resolution measurements[42] have found that the latter ratio is 1.3). We have carried out QCT calculations simulating the conditions of these HD experiments and found similar, but not nearly as dramatic results; these are shown in Fig. 9. The calculated OD product is more backward scattered than the OH by about a factor of 1.5, while the calculated OH is forward–backward symmetric, within the statistical uncertainty. The corresponding OH and OD translational energy distributions are shown in Fig. 10. These, too, have the same relative shapes as the experimental distributions (OD peaks at higher energy than OH), but they both peak around an energy approximately 5 kcal/mol higher than the experiment. The recent QCT calculations by Schatz and co-workers[33] show that accounting also for the contribution of the first excited PES $^1A''$, characterized by a barrier of 2.3 kcal/mol, provides a backward scattering contribution qualitatively in the direction of the experimental observation. A better agreement, although still not quantitative, with the experiment was noted by assuming that also the $2\,^1A'$ PES, having the same barrier of $^1A'$, contributes in an equal amount to the scattering.[33] However, very recent theoretical work by Schatz *et al.*[35] finds that the cross section on the $2\,^1A'$ surface is actually only about half that associated with the $^1A''$ surface, and product state distributions on the $2\,^1A'$ surface are intermediate in character between $1\,^1A'$ and $^1A''$.

V. DISCUSSION

When QCT results on the ground state DIM surface are compared with the experimental c.m. angular and translational energy distributions (Figs. 7 and 8), clear discrepancies are noted. In particular, while the experimental c.m. angular distributions exhibit a slight preference for backward scattering and are weakly polarized, the QCT angular distributions are nearly symmetric and somewhat more polarized. Better agreement is noted between calculated and experimental product translational distributions. In the case of $O(^1D)+HD$, only the trend of the experimental determination has been reproduced by the QCT calculations, while the detailed comparison has clear shortcomings. On the whole, QCT results on the ground state DIM PES do not reproduce the experiments exactly for any of the energies and isotopic variants examined; it was shown previously[32] that this is the case for the product vibrational distribution as well.

It is improbable that the above considered differences result from inadequacies in the accuracy of the ground $1\,^1A'$ potential energy surface since the new accurate calculations of this surface[26,27] have not indicated significant changes in its topology. The inclusion of the possibility for (Landau–Zener) surface hopping does not lead to an improved agreement between QCT results and experiment, since at these relatively low energies the probability for hopping is quite small, at least on this PES. Clearly, the failure of the QCT results on the DIM PES to adequately describe the experimental results is the consequence of deficiencies in the treatment of the excited potential energy surfaces. Specifically, the comparisons with the measured angular distributions suggest that the barrier on the excited state surface which gov-

erns the abstraction mechanism should be considerably lower than the value (3.7 kcal/mol) derived for $2\,^1A'$. The $2\,^1A'$ and $^1A''$ surfaces are both components of $^1\Pi$ for linear geometry near the saddle point and both may be involved at the energies of the experiments if the $^1\Pi$ state barrier is lower than 3.7 kcal/mol. Recently, Schatz and co-workers[35] compared the present DIM potential surfaces with their *ab initio* ground state and $^1A''$ surfaces; in particular, they pointed out that the $^1A''$ DIM surface has a barrier (the same of $2\,^1A'$) too high. They also compared the properties of the two exited $^1A''$ and $2\,^1A'$ surfaces within the DIM model which is able to account for couplings. The cross sections of the two excited surfaces are similar for energies close to the threshold, but at energies above the threshold the cross section for the $2\,^1A'$ surface is significantly reduced by the competition between surface hopping and barrier recrossing. Interestingly, they found that the $2\,^1A'$ product state distributions are intermediate between those of $^1A'$ and $^1A''$, since some of the trajectories that start on $2\,^1A'$ and hop to the $^1A'$ surface explore the H_2O well. In their *ab initio* calculations, the energy barrier for the $^1A''$ surface is 2.3 kcal/mol.[33] QCT calculations[33] for $O(^1D)+H_2$ at $E_c=2.7$ kcal/mol show that the $^1A'$ differential cross section is very nearly symmetric about $\theta=90°$, while that predicted by the $^1A''$ state is strongly backward peaked. The sum of the two contributions is a backward biased c.m. angular distribution (see Fig. 9 of Ref. 33). This result does not agree with that of the earlier crossed molecular beam study,[11] while is in line with what was found in the present study.

As can be seen from Fig. 7, in the case of $O(^1D)+H_2$ the preference for backward scattering is already visible at $E_c=1.9$ kcal/mol and increases slightly when going from $E_c=1.9$ to 3.0 kcal/mol. The observation of preferential backward scattering even at $E_c=1.9$ kcal/mol is more consistent with a barrier lower than 2.3 kcal/mol, such as the 1.5 kcal/mol value recently determined for the abstraction channel by Liu and co-workers[43] [the value of 1.8 kcal/mol reported in Ref. 43 includes the rotational energy (0.3 kcal/mol) of the H_2 reactant].

QCT calculations by Schatz and co-workers[56] for $O(^1D)+D_2$ at $E_c=5.3$ kcal/mol, including both the ground state and first excited $^1A''$ PES, find a branching ratio $\sigma_{abs}/\sigma_{ins}=0.22$. According to the experimentally derived energy dependence of the reactive integral cross section for the isotopic variants $O(^1D)+H_2/D_2/HD$, the ratio of the cross sections for abstraction and insertion, $\sigma_{abs}/\sigma_{ins}$, is about 0.5 for $O(^1D)+D_2$ at $E_c=5.3$ kcal/mol,[43] a value considerably larger than that determined by Schatz and co-workers.[56] A fit of the present $O(^1D)+D_2$ data at $E_c=5.3$ kcal/mol in terms of insertion and abstraction components gives $\sigma_{abs}/\sigma_{ins}\cong 0.17$, a value close to that predicted by the QCT calculations, if symmetric and backward peaked, respectively, angular distributions are used. However, preliminary experiments in our laboratory on $O(^1D)+H_2$ at $E_c=0.88$ kcal/mol indicate a slight preference for forward scattering at this low collision energy where only insertion is expected to occur, and this may imply that at higher energies insertion should be characterized by an increasingly more forward peaked angular distribution. This is not predicted by any QCT calculations to date. An analysis in terms of a forward peaked angular distribution for the insertion mechanism and a backward peaked angular distribution for the abstraction mechanism would lead to an increase of the ratio $\sigma_{abs}/\sigma_{ins}$, which would be in the direction of Liu's results.[43] Clearly, the ratio of cross sections for abstraction and insertion, and the relative importance of the two excited surfaces, $^1A''$ and $2\,^1A'$, for the abstraction mechanism are two aspects which warrant further theoretical and experimental investigation.

VI. CONCLUSION

The product vibrational and angular distributions of the $O(^1D)+H_2$ reaction are among the most sensitive indicators of the dynamics, and these have not been reproduced satisfactorily by any theoretical calculation made to date. Despite very refined computations of the lowest energy surface, this surface alone does not give enough vibrational excitation or enough backward scattering (for $E_c \geqslant 1.9$ kcal/mol) to reproduce the experiments. We conclude that additional channels must carry some of the reactive flux. This corroborates the conclusions of very recent work by Liu and co-workers,[41–43] who attribute the increasing backward scattering with increasing E_c to the onset of the abstraction mechanism for collinear encounters on the first excited PES. Of the five surfaces which are degenerate in the entrance channel, three are readily accessible at the energies of the present experiments: the first two $^1A'$ surfaces and the lowest $^1A''$ surface. Because of the high potential barrier, the $2\,^1A'$ surface of the DIM model does not contribute to the reactive scattering at the experimental energies of this work. The new *ab initio* $^1A''$ surface derived by Schatz and co-workers[33] has a lower barrier with respect to the DIM model and different topology with respect to $2\,^1A'$; it is expected to give significant contributions in the energy range of the present experiments, but this has not been examined here. However, the excited PES of Schatz and co-workers still underestimates[33] the backward scattering contribution for $O(^1D)+HD$ at $E_c=4.55$ kcal/mol, while slightly overestimates that observed in the present experiments for $O(^1D)+D_2$ at $E_c=5.3$ kcal/mol. Noticeably, other dynamical aspects of the $O(^1D)+H_2$, D_2, and HD reactions (as excitation functions and isotopic effects) are not well reproduced by QCT calculations using ground and excited surfaces. From the present work, however, we can conclude that QCT calculations which include insertion and abstraction contributions should be able to provide differential cross sections in semiquantitative agreement with our experimental observation. Recent QCT studies[35] on $O(^1D)+H_2$ predict that the backward scattering contribution from direct abstraction becomes more sideways distributed with increasing E_c, which is line with what is known about the dynamics of rebound reactions; therefore, the backward peak in the $O(^1D)+D_2$ angular distribution is not expected to become significantly more intense for E_c higher than 5.3 kcal/mol, but rather to broaden. Indeed, preliminary measurements in our laboratory at $E_c=6.1$ kcal/mol appear to corroborate this expectation.

The cross sections on the excited state surfaces, and hence their contribution to the overall product distributions are a sensitive function of the energy barriers, and of the nonadiabatic couplings between the various surfaces, neither of which is well known. It is desirable to have refined computations of these surfaces so the barriers may be better determined and nonadiabatic coupling included in the dynamic calculations. We will carry out more experiments, hopefully backed up by suitable dynamical calculations, to establish whether the details of the scattering distributions can give information about the relative contributions of the two excited surfaces. Presently, however, the possibility remains that both give substantial contributions to the cross section of this reaction. Finally, in order to carry out unambiguous tests of the PES and verify the reliability of the QCT calculations, exact quantum scattering computations are desirable and may become feasible in the near future.

ACKNOWLEDGMENTS

We wish to acknowledge G. C. Schatz, K. Liu, A. Suits, and J. P. Simons for valuable discussions, preprints, and provision of some of their unpublished data. We are grateful to D. Stranges for his help during the early stages of this project. This work was supported by the Italian ''Consiglio Nazionale delle Ricerche—Progetto Finalizzato Chimica Fine'' and ''Ministero Universitàe Ricerca Scientifica,'' by grants from NATO (CRG 920549) and the Air Force Office of Scientific Research (Grant No. F617-08-94-C-0013) through the European Office of Aerospace Research and Development (Grant No. SPC-94-4042), and by the Natural Sciences and Engineering Research Council of Canada.

[1] G. K. Smith, J. E. Butler, and M. C. Lin, Chem. Phys. Lett. **65**, 115 (1979).
[2] A. C. Luntz, J. Chem. Phys. **73**, 1144 (1980).
[3] G. K. Smith and J. E. Butler, J. Chem. Phys. **73**, 2243 (1980).
[4] J. E. Butler, R. G. MacDonald, D. J. Donaldson, and J. J. Sloan, Chem. Phys. Lett. **95**, 183 (1983).
[5] P. M. Aker and J. J. Sloan, J. Chem. Phys. **85**, 1412 (1986).
[6] G. M. Jurisch and J. R. Wiesenfeld, Chem. Phys. Lett. **119**, 511 (1985).
[7] L. Holmlid and K. Rynefors, Chem. Phys. **60**, 393 (1981).
[8] K. Rynefors and L. Holmlid, Chem. Phys. **60**, 405 (1981).
[9] K. Rynefors, P.-A. Elofson, and L. Holmlid, Chem. Phys. **100**, 53 (1985).
[10] P.-A. Elofson, K. Rynefors, and L. Holmlid, Chem. Phys. **100**, 395 (1985).
[11] R. Buss, P. Casavecchia, T. Hirooka, S. J. Sibener, and Y. T. Lee, Chem. Phys. Lett. **82**, 386 (1981).
[12] J. E. Butler, G. M. Jurisch, I. A. Watson, and J. R. Wiesenfeld, J. Chem. Phys. **84**, 5365 (1986).
[13] C. B. Cleveland, G. M. Jurisch, M. Trolier, and J. R. Wiesenfeld, J. Chem. Phys. **86**, 3253 (1987).
[14] K. Mikulecky and K.-H. Gericke, J. Chem. Phys. **96**, 7490 (1992).
[15] K. Mikulecky and K.-H. Gericke, Chem. Phys. **175**, 13 (1993).
[16] Y. Huang, Y. Gu, C. Liu, X. Yang, and Y. Tao, Chem. Phys. Lett. **127**, 432 (1986).
[17] A. C. Luntz, R. Schinke, W. A. Lester, Jr., and Hs. H. Gunthard, J. Chem. Phys. **70**, 5908 (1979).
[18] P. A. Whitlock, J. T. Muckerman, and P. M. Kroger, *Potential Energy Surfaces and Dynamics Calculations*, edited by D. G. Truhlar (Plenum, New York, 1981).
[19] P. A. Whitlock, J. T. Muckerman, and E. R. Fisher, J. Chem. Phys. **76**, 4468 (1982).
[20] M. S. Fitzcharles and G. C. Schatz, J. Phys. Chem. **90**, 3634 (1986).
[21] E. M. Goldfield and J. R. Wiesenfeld, J. Chem. Phys. **93**, 1030 (1990).
[22] J. K. Badenhoop, H. Koizumi, and G. C. Schatz, J. Chem. Phys. **91**, 142 (1989).
[23] T. Peng, D. H. Zhang, J. Z. H. Zhang, and R. Schinke, Chem. Phys. Lett. **248**, 37 (1996).
[24] R. Schinke and W. A. Lester, J. Chem. Phys. **72**, 3754 (1980).
[25] J. N. Murrell and S. Carter, J. Phys. Chem. **88**, 4887 (1984); J. N. Murrell, S. Carter, I. M. Mills, and M. F. Guest, Mol. Phys. **42**, 605 (1981); K. S. Sorbie and J. N. Murrell, *ibid.* **29**, 1387 (1975).
[26] Tak-San Ho, T. Hollebeek, H. Rabitz, L. B. Harding, and G. C. Schatz, J. Chem. Phys. **105**, 10,472 (1996).
[27] A. J. C. Varandas, J. Chem. Phys. **105**, 3524 (1996).
[28] A. J. C. Varandas, A. I. Vovonin, A. Riganelli, and P. J. S. B. Caridade, Chem. Phys. Lett. **278**, 325 (1997).
[29] The surface is an extension of that described in R. Polák, K. Paiderová, and P. J. Kuntz, J. Chem. Phys. **87**, 2863 (1987), containing improvements in several details relating to the long range forces and the $H_2O(X\ ^1A_1)$ minimum. The same surface was used in Refs. 30–32.
[30] P. J. Kuntz, B. I. Niefer, and J. J. Sloan, J. Chem. Phys. **88**, 3629 (1988).
[31] P. A. Berg, P. J. Kuntz, and J. J. Sloan, J. Chem. Phys. **95**, 8038 (1991).
[32] P. J. Kuntz, B. I. Niefer, and J. J. Sloan, Chem. Phys. **151**, 77 (1991).
[33] G. C. Schatz, A. Papaioannou, L. R. Harding, T. Hollebeek, T.-S. Ho, and H. Rabitz, J. Chem. Phys. **107**, 2340 (1997).
[34] A. J. C. Varandas, J. Chem. Phys. **107**, 867 (1997).
[35] G. C. Schatz, L. A. Pederson, and P. J. Kuntz, Faraday Discuss **108** (1997).
[36] J. A. Davidson, C. M. Sadowski, H. I. Schiff, G. E. Streit, C. J. Howard, D. A. Jennings, and A. L. Schmeltekopf, J. Chem. Phys. **64**, 57 (1976); J. A. Davidson, H. I. Schiff, G. E. Streit, J. R. McAfee, A. L. Schmeltekopf, and C. J. Howard, *ibid.* **67**, 5021 (1977).
[37] W. B. DeMore, S. P. Sander, D. M. Golden, R. F. Hampson, M. J. Kurylo, C. J. Howard, A. R. Ravishankara, C. E. Kolb, and M. J. Molina, *Chemical Kinetics and Photochemical Data for Use in Stratospheric Modelling*, JPL publication 94-26 (Jet Propulsion Laboratory, Pasadena CA, 1994).
[38] R. K. Talukdar and A. R. Ravishankara, Chem. Phys. Lett. **253**, 177 (1996).
[39] T. Laurent, P. D. Naik, H.-R. Volpp, J. Wolfrum, T. Arusi-Parpar, I. Bar, and S. Rosenwaks, Chem. Phys. Lett. **236**, 343 (1995); S. Koppe, T. Laurent, P. D. Naik, H.-R. Volpp, J. Wolfrum, T. Arusi-Parpar, I. Bar, and S. Rosenwaks, *ibid.* **214**, 546 (1993).
[40] Y. Matsumi, K. Tonokura, M. Kawasaki, and H. L. Kim, J. Phys. Chem. **96**, 10,622 (1992); K. Tsukiyama, B. Katz, and R. Bersohn, J. Chem. Phys. **83**, 2889 (1985).
[41] D.-C. Che and K. Liu, J. Chem. Phys. **103**, 5164 (1995).
[42] Y.-T. Hsu and K. Liu, J. Chem. Phys. **107**, 1664 (1997).
[43] Y.-T. Hsu, J.-H. Wang, and K. Liu, J. Chem. Phys. **107**, 2351 (1997).
[44] A. J. Alexander, F. J. Aoiz, M. Brouard, I. Burak, Y. Fujimura, J. Short, and J. P. Simons, Chem. Phys. Lett. **262**, 589 (1996).
[45] A. J. Alexander, F. J. Aoiz, M. Brouard, and J. P. Simons, Chem. Phys. Lett. **256**, 561 (1996).
[46] A. G. Suits (private communication).
[47] M. Alagia, N. Balucani, P. Casavecchia, D. Stranges, and G. G. Volpi, J. Chem. Soc., Faraday Trans. **91**, 575 (1995).
[48] P. Casavecchia, N. Balucani, and G. G. Volpi, in Adv. Ser. Phys. Chem. Vol. 6, edited by K. Liu and A. Wagner (World Scientific, Singapore, 1995), Ch. 9.
[49] M. Alagia, V. Aquilanti, D. Ascenzi, N. Balucani, D. Cappelletti, L. Cartechini, P. Casavecchia, F. Pirani, G. Sanchini, and G. G. Volpi, Isr. J. Chem. **37**, 329 (1997).
[50] N. Balucani, L. Beneventi, P. Casavecchia, D. Stranges, and G. G. Volpi, J. Chem. Phys. **94**, 8611 (1991); N. Balucani, L. Beneventi, P. Casavecchia, and G. G. Volpi, Chem. Phys. Lett. **180**, 34 (1991); N. Balucani, P. Casavecchia, D. Stranges, and G. G. Volpi, *ibid.* **211**, 469 (1993); N. Balucani, L. Beneventi, P. Casavecchia, G. G. Volpi, E. J. Kruus, J. J. Sloan, Can. J. Chem. **72**, 888 (1994); M. Alagia, N. Balucani, P. Casavecchia, A. Lagana, G. Ochoa de Aspuru, E. H. van Kleef, G. G. Volpi, and G. Lendway, Chem. Phys. Lett. **258**, 323 (1996); M. Alagia, N. Balucani, P. Casavecchia, D. Stranges, G. G. Volpi, D. C. Clary, A. Kliesch, and H.-J. Werner, Chem. Phys. **207**, 389 (1996); M. Alagia, N. Balucani, P. Casavecchia, and G. G. Volpi, J. Phys. Chem. A **101**, 6455 (1997).
[51] M. Alagia, N. Balucani, L. Cartechini, P. Casavecchia, E. H. van Kleef, G. G. Volpi, F. J. Aoiz, L. Bañares, D. W. Schwenke, T. C. Allison, S. L. Mielke, and D. G. Truhlar, Science **273**, 1519 (1996).

[52] S. J. Sibener, R. J. Buss, C. Y. Ng, and Y. T. Lee, Rev. Sci. Instrum. **51**, 167 (1980).
[53] J. E. Pollard, D. J. Trevor, Y. T. Lee, and D. A. Shirley, J. Chem. Phys. **77**, 4818 (1982).
[54] K. Sköld, Nucl. Instrum. Methods **63**, 114 (1968).
[55] K. Liu (private communication).
[56] G. C. Schatz (private communication); see also: P. Casavecchia, M. Alagia, N. Balucani, L. Cartechini, E. H. van Kleef, G. G. Volpi, L. Harding, H. Rabitz, T. Hollebeek, T.-S. Ho, L. A. Pederson, and G. C. Schatz, Faraday Discuss. **108** (1997).